

## High Sensitivity Gravitational Wave Antenna with Parametric Transducer Readout

D. G. Blair, E. N. Ivanov, M. E. Tobar, P. J. Turner, F. van Kann, and I. S. Heng  
*Physics Department, University of Western Australia, Nedlands, Western Australia, 6009*  
 (Received 4 April 1994; revised manuscript received 27 September 1994)

A high- $Q$  niobium resonant mass gravitational radiation antenna with a superconducting parametric transducer and noncontacting readout is shown to achieve a noise temperature of about 2 mK using a zero order predictor filter. The predicted intrinsic cold damping of a parametric transducer is confirmed, along with predicted backaction limits on the sensitivity. While the antenna has the highest intrinsic  $Q$  factor and lowest noise temperature ever observed in a full scale antenna, the possibility of further improvements is demonstrated.

PACS numbers: 95.55.Ym, 04.80.Nn

Resonant mass gravitational wave antennas have been painstakingly improved over the past 20 years [1,2]. Cryogenic operation, superconducting transducers, improved vibration isolation, and increased acoustic  $Q$  factors have contributed to a  $10^4$ -fold improvement in energy sensitivity over Weber's original antennas [3]. Two types of superconducting transducers have been developed: SQUID based inductive or capacitive sensors [4] and parametric transducers utilizing radio frequency [5] or microwave resonators [6]. Although the latter devices have been promoted as potentially very sensitive transducers, they have not previously been successfully implemented in a full scale antenna. The problems encountered included the possibility of the transducer causing parametric excitations of the antenna [7], excess noise due to the microwave readout electronics, and the effects of low frequency seismic noise.

In this Letter we report the first successful operation of a large scale cryogenic resonant mass antenna instrumented with a superconducting parametric transducer. We show that the system achieves a noise temperature of less than 2 mK, representing a threefold noise energy sensitivity over SQUID based systems operated to date. Parametric instability of the antenna is avoided by controlled operation in the cold damped regime where the mean energy of antenna displacement fluctuations is about 10 times less than the equilibrium value. The noise in the readout electronics is reduced by using a 10 GHz sapphire loaded superconducting cavity oscillator [8] with the lowest ever measured phase noise at 1 kHz [9], and cryogenic microwave amplification employing an active carrier suppression technique [10]. The effect of seismic noise is greatly reduced by an improved cryogenic vibration isolation system [11] and a noncontacting microwave coupling to the transducer [12].

Figure 1 shows a simplified diagram of the antenna. It operates at about 5 K, and consists of a 1.5 ton Nb bar with a fundamental frequency of 710 Hz bonded to a 0.45 kg Nb bending flap with a resonant frequency of 700 Hz. The observed coupled frequencies are at 713 Hz (barlike mode) and 694 Hz (flaplike mode). The bending flap acts as a

mechanical amplifier impedance transformer to match the antenna impedance to the mechanical impedance of the transducer [13].

The vibrational state of the niobium bar is continuously monitored by a superconducting reentrant cavity whose capacitance is modulated by the relative motion of the bar and the bending flap. The low-noise microwave pump signal is coupled radiatively to the transducer by two

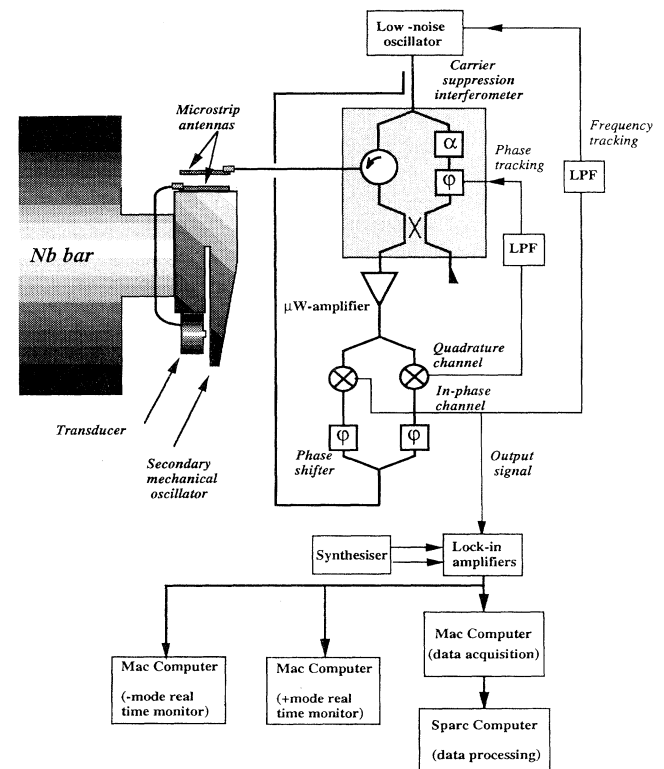


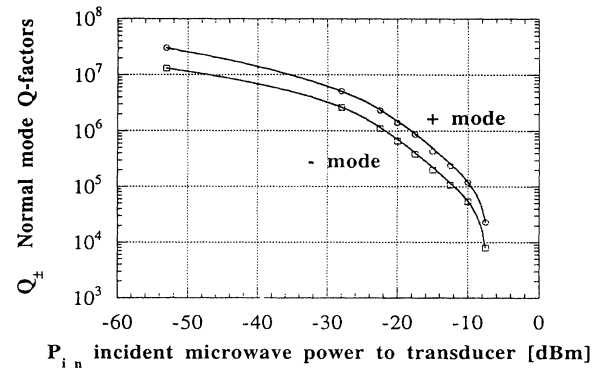
FIG. 1. Diagram of the antenna and transducer system. The carrier suppression interferometer and the microwave amplifier are located in the cryogenic environment. The frequency and phase tracking servos are shown schematically. The monitor computers display the data in real time, and plot histograms for up to 24 h operation.

miniature microstrip antennas [11]. These eliminate the need for any wiring connection between the transducer and its associated electronics, allowing the highest possible mechanical isolation of the antenna from the environment. The signal from the transducer is processed in a phase sensitive microwave signal processing circuit (MSPC), comprising an active carrier suppression interferometer, a cryogenic amplifier, and a room temperature mixer. The carrier suppression interferometer is a key element of the MSPC which allows low-noise cryogenic amplification of the extremely weak signal reflected from the transducer. Two servo control systems provide stable operation of the MSPC. The first servo maintains a constant negative offset between the pump source and transducer resonant frequency. This is required to maintain parametric cold damping (see below), and it also suppresses variations of the transducer resonant frequency caused by low frequency seismic excitation of the normal modes in the vibration isolation system. The second servo maintains the carrier suppression interferometer locked to the "dark fringe" despite the low frequency rocking motions of the bar, which causes path length variations in the non-contacting coupling.

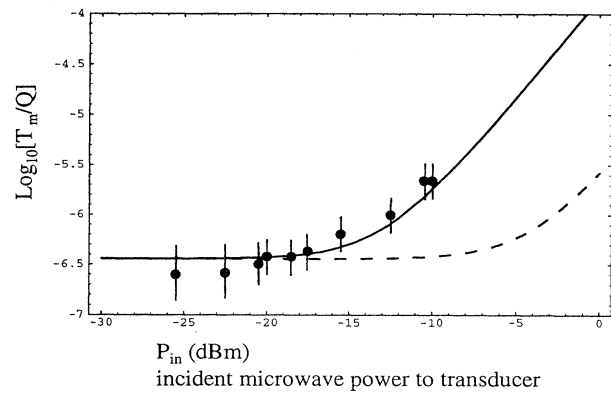
The interaction of the parametric transducer with the resonant bar causes changes in the resonant frequency and in the  $Q$  factor of the antenna normal modes [14,15]. Experimental observations of this effect are shown in Fig. 2(a). The unperturbed  $Q$  factors measured at a very low transducer input power ( $P_{in} = -45$  dBm at 10 GHz) are equal to  $3 \times 10^7$  and  $1.3 \times 10^7$  for the barlike mode (713 Hz) and the flaplike mode (694 Hz), respectively. As the microwave power is increased, nondissipative parametric cold damping causes the  $Q$  factor to reduce, as shown in Fig. 2(a).

The energy of the displacement fluctuations of the flap at the frequencies of the normal modes can be expressed in terms of the mode temperature  $T_m$ . At  $P_{in} = -45$  dBm,  $T_m$  is equal (within experimental error) to the physical temperature of the antenna (about 5 K), consistent with the expected Brownian motion in the antenna. However, the cold damping which reduces the  $Q$  factors also reduces the mode temperature. At low power levels the cold damping preserves the ratio  $T_m/Q$  [Fig. 2(b)], which confirms the intrinsic cold damped operation of the transducer. At higher power levels the ratio  $T_m/Q$  increases proportionally to  $P_{in}^2$ . This occurs due to increased backaction noise which arises from pump oscillator amplitude noise which produces fluctuations in the attractive force acting between the transducer and antenna. In the low power regime the antenna sensitivity increases with  $P_{in}$ . However, in the backaction regime the sensitivity decreases. Thus the antenna-transducer system is characterized by a classical uncertainty relation for which there is an optimum input power and integration time.

For measuring the antenna noise temperature  $T_n$  we use a pair of lock-in amplifiers centered on the antenna normal



(a)



(b)

FIG. 2. (a) Dependence of the acoustic quality factor on the input power to the transducer, showing the parametric cold damping at higher power levels. (b) Dependence of the  $T/Q$  ratio of the minus mode on the input power to the transducer. The points are experimental measurements and the lines are theoretical calculations. The bold curve represents the  $T/Q$  ratio for the present configuration. If the pump amplitude noise was reduced from  $-140$  to  $-160$  dBc/Hz, the breakpoint would shift to  $-3$  dBm (dashed curve). The optimum sensitivity occurs at the breakpoint when the input power is  $-12$  dBm. Below  $-12$  dBm the system operated in the nondissipative cold damped regime where  $T/Q$  remains constant. Above  $-12$  dBm the amplitude noise acts back on the oscillator, degrading the  $T/Q$  ratio proportionally to  $P_{in}^2$ .

modes, and a zero order prediction (ZOP) algorithm based on this two channel synchronous detection system [16]. When properly tuned this algorithm achieves a signal-to-noise ratio only 2.3 times less than an ideal optimal filter [17]. The noise temperature is determined by fitting the observed energy distribution of the voltage noise at the filter output to a Boltzmann distribution. The conversion from displacement to electrical units is determined from the known transducer tuning coefficient  $df/dx$  and the measured transducer  $Q$  factor. A reproducible exponential behavior is achieved, with a low level of excess high energy events, as shown in Fig. 3(a).

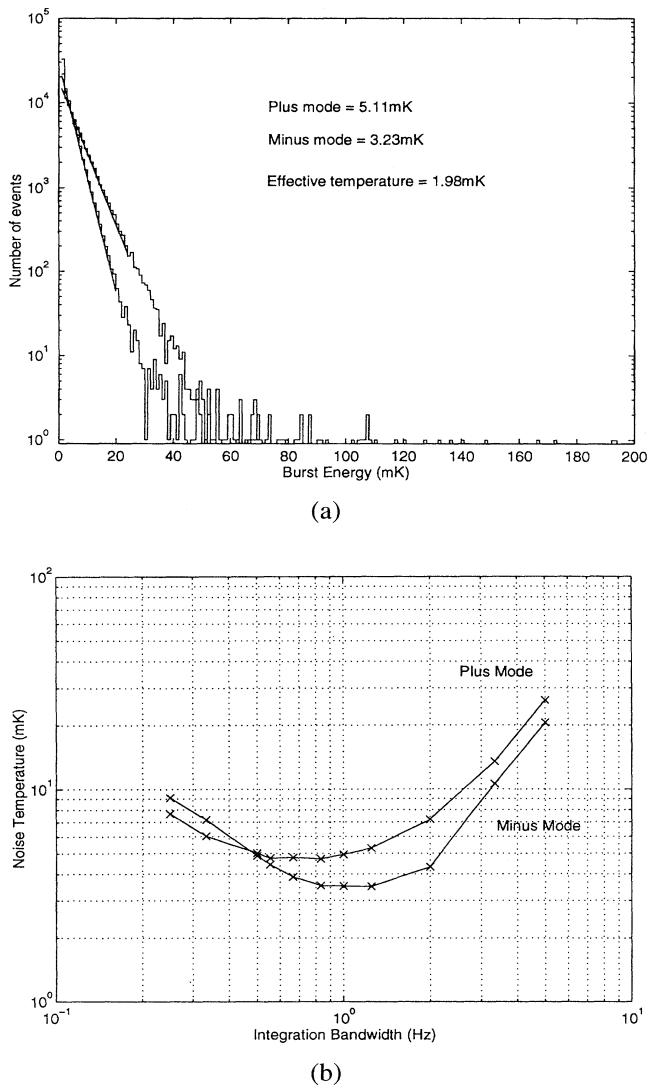


FIG. 3. (a) Effective energy histogram for day 234, 1994, using a ZOP filter. The histograms show expected Gaussian behavior with no more than 60 non-Gaussian “events” in the high energy tail. (b) The effective temperature dependence on integration bandwidth for the two antenna normal modes. The data are sampled at 10 Hz, and then correctly filtered, decimated, and plotted a histogram to obtain each data point. MATLAB routines are used for the data processing.

Noise temperature measurements for each mode of the antenna versus sampling time are shown in Fig. 3(b) for the data of day 234, 1994. A minimum in  $T_n$  occurs when contributions from the narrow band noise (Brownian motion and backaction noise) and the broad band noise (additive noise of the readout electronics) are equal. The antenna bandwidth  $\Delta f$  is the reciprocal of the sampling time at which the minimum of  $T_n$  is achieved. To calculate the overall noise temperature of the antenna we use the relation  $1/T_n = 1/T_{n(713)} + 1/T_{n(694)}$ . This gives a detector

noise temperature of 2 mK. Thus with our present scheme we expect the antenna to operate at a noise temperature of about 1 mK when the optimal filter is implemented. This result is consistent with a detailed mathematical model of the detector [18]. At optimum power the broad band noise is  $3 \times 10^{-17} \text{ m}/\sqrt{\text{Hz}}$  (referenced to the bending flap). This noise is entirely due to the microwave amplifier. The narrow band noise is  $6 \times 10^{-26} \text{ N}^2/\text{Hz}$  for a cold damped mode temperature of 0.5 K.

From Fig. 3 the bandwidth of our antenna is about 1 Hz, which is less than optimum because the bar and flap are detuned by 10 Hz. This is consistent with our model, which also predicts that more accurate tuning would improve the bandwidth by up to a factor of 3. Note, however, that detuning affects the strain sensitivity only to second order. Electronic tuning can be achieved by exploiting the parametric interactions of the transducer with the bending flap, but only if the flap mode frequency is above the bar frequency (which is not the present case) [13]. To increase the bandwidth and sensitivity for the existing antenna configuration, both series and backaction noise must be reduced. Both noise sources are believed to be due to amplitude noise in the pump oscillator. Power stabilization schemes are expected to reduce the series noise from  $5 \times 10^{-17}$  to  $1.5 \times 10^{-18} \text{ m}/\sqrt{\text{Hz}}$  by suppressing the oscillator AM noise from  $-140$  to  $-160 \text{ dBc/Hz}$  (in the latter case the power of AM fluctuations measured at 700 Hz offset from the carrier in 1 Hz bandwidth is 160 dB less than the carrier power). The model shows that for  $P_{\text{in}} = -3 \text{ dBm}$ , the noise temperature is reduced to  $30 \mu\text{K}$ , corresponding to a 1 ms burst strain sensitivity of  $10^{-19}$  with a bandwidth of about 10 Hz. If the bar and the flap were tuned properly, the bandwidth would be increased to about 20 Hz. Except for the tuning, these improvements can be implemented without interrupting long term operation. The antenna is now participating in a long term coincidence experiment with the cryogenic Al bars of the LSU and Rome groups.

We would like to thank Dr. A.G. Mann, Dr. P.J. Veitch, and Dr. N.P. Linthorne for their contribution toward the success of this experiment, and Dr. C. Edwards and Professor M.J. Buckingham for their long term support. This work would have been impossible without the outstanding contributions of our workshop staff and was supported by the Australian Research Council.

- [1] W.O. Hamilton, in *Proceedings of the Sixth Marcel Grossmann Meeting on General Relativity* (World Scientific, Singapore, 1992), p. 988.
- [2] P. Astone *et al.*, in *Gravitational Astronomy: Instrument Design and Astrophysical Prospects*, edited by D.E. McClelland and H.A. Bachor (World Scientific, Singapore, 1991), p. 189.
- [3] J. Weber, *Phys. Rev.* **117**, 306 (1960).
- [4] P.F. Michelson and R.C. Taber, *J. Appl. Phys.* **52**, 4313 (1981).

- [5] M.F. Bocko and W.W. Johnson, Phys. Rev. A **30**, 2135 (1984).
- [6] P.J. Veitch, D.G. Blair, N.P. Linthorne, L.D. Mann, and D.K. Ramm, Rev. Sci. Instrum. **58**, 1910 (1987).
- [7] V.B. Braginsky and A.B. Manukin, in *Measurement of Weak Forces in Physics Experiments* (University of Chicago Press, Chicago, 1977), p. 19.
- [8] A.J. Giles, S.K. Jones, D.G. Blair, and M.J. Buckingham, in *Proceedings of the 43rd Annual Symposium of Frequency Control* (IEEE, Piscataway, NJ, 1989), p. 89.
- [9] M.E. Tobar and D.G. Blair, IEEE Trans. Microwave Theory Tech. **42**, 344 (1994).
- [10] E.N. Ivanov, P.J. Turner, and D.G. Blair, Rev. Sci. Instrum. **64**, 3191 (1993).
- [11] D.G. Blair *et al.*, in *Some New Trends on Fluid Mechanics and Theoretical Physics*, edited by C.C. Lin and Ning Hu (Peking University Press, Beijing, 1993), p. 591.
- [12] E.N. Ivanov, M.E. Tobar, P.J. Turner, and D.G. Blair, Rev. Sci. Instrum. **64**, 1905 (1993).
- [13] H.J. Paik, Ph.D. thesis, Stanford University, 1974.
- [14] N.P. Linthorne, P.J. Veitch, and D.G. Blair, J. Phys. D **23**, 1 (1990).
- [15] M.E. Tobar and D.G. Blair, J. Phys. D **26**, 2276 (1993).
- [16] G.V. Pallottino and G. Pizella, in *Detection of Gravitational Waves*, edited by D.G. Blair (Cambridge University Press, Cambridge, 1991), p. 242.
- [17] G.V. Pallottino, in *Gravitational Radiation, Collapsed Objects and Exact Solutions*, edited by J. Ehlers *et al.*, Lecture Notes in Physics Vol. 124 (Springer-Verlag, Berlin, 1980).
- [18] M.E. Tobar and D.G. Blair (to be published).

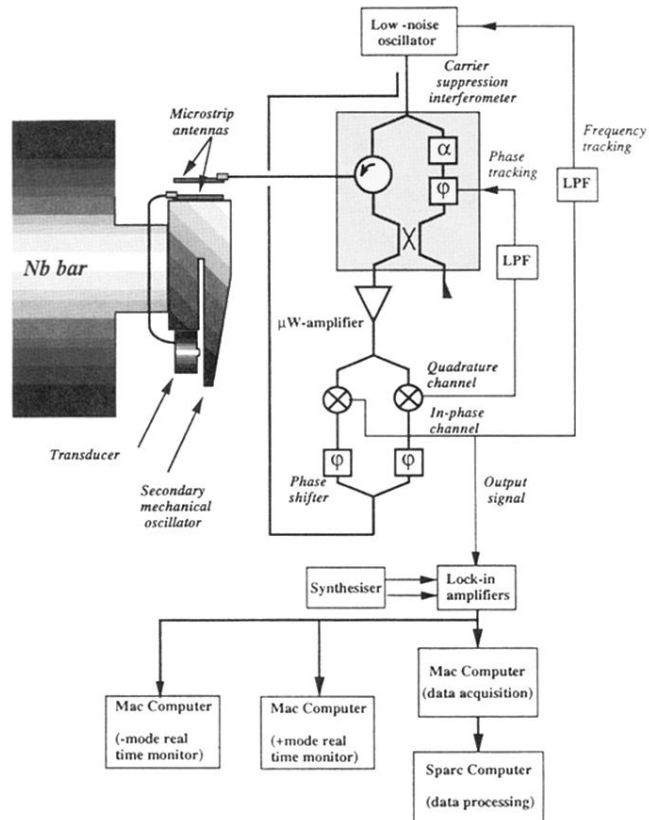


FIG. 1. Diagram of the antenna and transducer system. The carrier suppression interferometer and the microwave amplifier are located in the cryogenic environment. The frequency and phase tracking servos are shown schematically. The monitor computers display the data in real time, and plot histograms for up to 24 h operation.